ON THE STABILITY OF HOMOGENEOUS SOLUTIONS TO SOME AGGREGATION MODELS

R. Kowalczyk, A. Gamba and L. Preziosi

Department of Mathematics, Politecnico
Torino, Italy
kowalcz@calvino.polito.it, gamba@polito.it, luigi.preziosi@polito.it

ABSTRACT. Vasculogenesis, *i.e.* self-assembly of endothelial cells leading to capillary network formation, has been the object of many experimental investigations in recent years, due to its relevance both in physiological and in pathological conditions. We performed a detailed linear stability analysis of two models of *in vitro* vasculogenesis, with the aim of checking their potential for structure formation starting from initial data representing a continuum cell monolayer. The first model turns out to be unstable at low cell densities, while pressure stabilizes it at high densities. The second model is instead stable at low cell densities. Detailed information about the instability regions and the structure of the critical wave numbers are obtained in several interesting limiting cases. We expect that altogether, this information will be useful for further comparison of the two models with experiments.

1. **Introduction.** In living beings, complex structures arise from the aggregation of separate constituents. A typical example is given by the formation of the vascular network in vertebrates, where vascular endothelial cells migrate over long distances and finally coalesce to form complex vascular structures [11, 7]. The process takes place during the early stages of embryo development and is therefore difficult to observe in its dynamical details. To circumvent this difficulty, several *in vitro* assays have been devised [4]. In the experiments, cells are randomly seeded on the plain surface of a gel substratum and their migration and aggregation observed through videomicroscopy. In this way, the process of formation of a capillary-like network can be accurately tracked [1]. Tracking of individual trajectories shows marked persistence in the direction of cell motion, with a small random component superimposed. Cells migrate over distances which are an order of magnitude larger than their radius and stick together when they get in contact with their neighbours. Motion is apparently directed towards zones of higher cell concentration, suggesting that chemotactic factors play a relevant role in the process. In a time of the order of some hours cells form a continuous multicellular network which can be described as a collection of nodes connected by chords (Fig. 1a). It is experimentally observed that *i)* the mean chord length $\bar{l}$ is approximately independent on the initial cell density ($\bar{l} \simeq 200 \pm 20 \mu$m); *ii)* connected networks are formed only above a critical density $n_c \sim 100$ cells/mm^2 (a phenomenon known as a percolative transition [12]); *iii)* at higher cell densities the chord thickness grows in order to accommodate a larger number of cells (Fig. 1b), until around 400 cells/mm^2, a sort of

---

"Swiss-cheese" structure is observed (Fig. 1c). The experimental system therefore presents three different regimes, depending on the assigned value of the initial cell density n: $a)$ a low density phase where one observes only the formation of isolated clusters; $b)$ an intermediate density phase where clearly defined capillary-like networks are formed (Fig. 1a); $c)$ a high density phase characterized by "Swiss cheese" patterns like those shown in Fig. 1b,c. The transition between phase $a)$ and $b)$ is sharp, $i.e.$, characterized by a well defined critical density n_c. This allows to use known methods of statistical mechanics to characterize it quantitatively through the computation of a set of critical indices [5]. The transition between phase $b)$ and $c)$ is instead a continuum crossover, characterized by the accumulation of an ever increasing number of cells on the network chords, until at very high densities the network itself ceases to be recognizable. At high cell densities, the randomly seeded cells form in the initial moments of the experimental sessions an almost continuous monolayer. Cells are then seen to aggregate, as if an attractive force were drawing them together, and large holes as those shown in Figs. 1b, c, are formed.[1]

The dynamics of vasculogenesis is apparently dictated by a program encoded in the cell genes that leads them to respond to different stimuli and to different environments in precise ways. Isolated cells in contact with the proteins of the substratum seem to have been programmed to perform migration towards zones of higher cell concentrations, presumably being guided by chemotactic gradients. However, when cells get in mutual contact a different program starts, commanding the formation of adhesive contacts among the cells and with the substratum, and the activation of traction forces. Generally speaking, there are several factors affecting the movement of endothelial cells. Among them are: $i)$ chemotaxis, where a chemical gradient can direct migration both up and down a concentration gradient; $ii)$ haptotaxis, where the cells move up towards denser zones of the substratum; $iii)$ convection, where cells are passively carried by the deforming substratum; $iv)$ contact guidance in which the substratum on which the cells crawl suggests a preferred direction; $v)$ contact inhibition by the cells, where a high density of neighboring cells inhibits motion.

In [5] a model for the early stages of vasculogenesis has been proposed. The model takes into account migration and chemotaxis and is able to reproduce several experimentally observed facts: $i)$ the formation of network structures starting from realistic initial data which mimic a set of randomly seeded cells initially at rest ($cf.$ Fig. 1d); $ii)$ the correct network size $\bar{l} \simeq 200\mu$m, predicted by the model as a function of physically measurable quantities; $iii)$ the percolative transition around $n_c \sim 100$ cells/mm^2; $iv)$ the formation of the "Swiss-cheese" phase at high densities ($cf.$ Figs. 1e-f); $v)$ the fractal dimension D_H of network structures both at small ($D_H = 1.50 \pm 0.02$) and large scales ($D_H = 1.87 \pm 0.03$); $vi)$ the set of experimentally observed critical indices.

A different model, not taking into account chemotaxis and focusing on the interaction of the cells with the substratum, has been proposed in [10]. In this model, along with the cell density, the main variable considered is the density of the underlying substratum. Cell movement is assumed to be due to two mechanisms: $i)$

---

[1]It is interesting to notice that such patterns have been observed in mice characterized by severe vascularization diseases, see the discussion in [1].
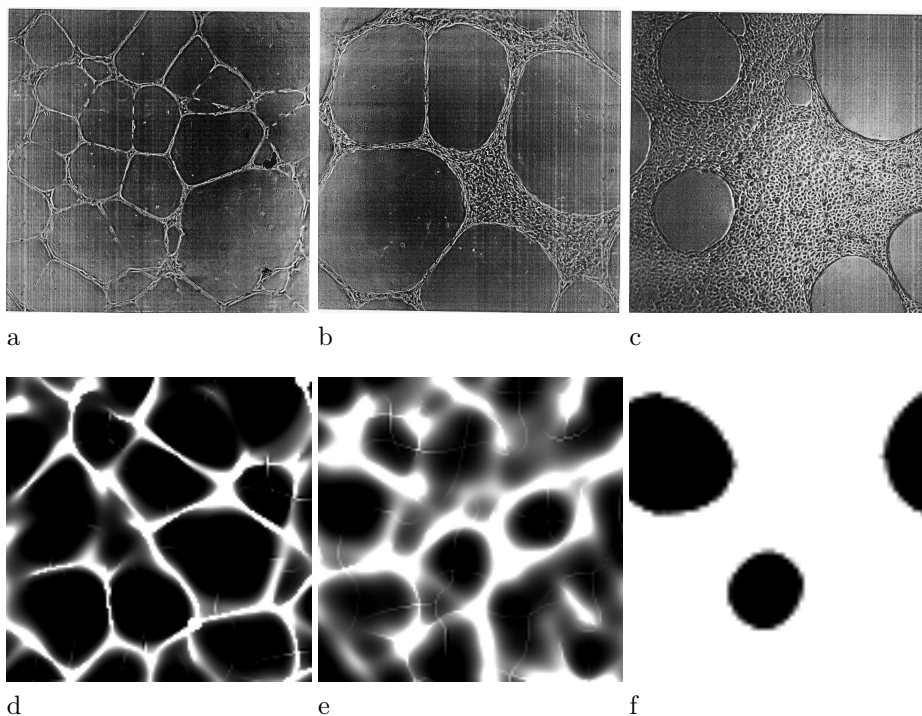
FIGURE 1. a-c: Types of capillary-like networks formed by plating different number of cells ($\bar{n} = 250$, 500, 1000 cells/mm^2) in a Petri dish covered with a substratum favoring the growth of a vascular-type network (experimental pictures kindly provided by F. Bussolino and G. Serini). d-f: Results of numerical simulations of the model introduced in [5], using measured values of the physical parameters and initial conditions mimicking the initial random placement of cells.

passive transport due to the motion of the substratum, and *ii)* diffusion on the substratum itself.[2] The cells are assumed to exert traction forces on the substratum, which are modeled through a phenomenological coupling relating the substratum stress tensor to the cell density n. The model was simulated in [10] using as initial condition a small perturbation over a uniform background distribution of cell density, which physically corresponds to a continuous cell monolayer, characterized by small inhomogeneities.

It seems reasonable that the two models provide somehow complementary descriptions of the vasculogenesis process. Model [5] has been shown to successfully describe early, migration dominated stages of network formation. Model [10] apparently contains some of the ingredients which are necessary to describe later, strain-dominated stages. In this paper, along with the model introduced in [5], we consider a somehow generalized isotropic version of the model introduced in [10], where we consider some additional effects: *i)* a relaxation term in the equation for

---

[2]The diffusion term is assumed to model cells random walk (possibly biased towards zones of highest strain of the substratum), therefore the right interpretation for n should be that of a probability density, instead of a real cell density.

the elastic restoring force of the substratum; *ii)* a general functional form for the stress exerted by cells; *iii)* a general functional form for the drag exerted by the substratum as a function of the substratum thickness. In what follows, we shall refer to the model of [5] as "Model I" and to our version of the model introduced in [10] as "Model II".

The main characteristic of both models is the emergence of structured patterns out of random or uniform initial conditions. The emergence of patterns starting from low and intermediate density initial conditions, in the neighborhood of the percolative transition, has been addressed in Refs. [5, 1]. Here we study in more analytical detail the emergence of patterns starting from the high density phase (*cf.* Figs. 1c), physically corresponding to almost continuous cell monolayers. These initial states are conveniently modeled as uniform density distributions with small, random inhomogeneities which can be seen as perturbations around a constant background. It is well known that the onset of structured patterns in extended systems can be traced back to the existence of spatially structured modes which are reinforced by the dynamics [9, 14]. The initial growth of such modes can be studied by means of a linear stability analysis. It appears then natural to apply this kind of analysis to the previously discussed vasculogenesis models, in order to study the process of pattern formation starting from quasi-uniform (monolayer type) initial conditions

We performed such a stability analysis for both Model I and II. We obtained detailed information about the regions of instability and the critical wave numbers for both models.

In model I we observed that the onset of instabilities is depressed by the effect of pressure forces. For high enough densities the uniform steady state is stable with respect to perturbations at all wavelengths. Lowering the density values one observes the onset of long wavelength instabilities, with a cutoff at small wavelengths. The main instability is a function of pressure which reaches a limiting value for zero pressure. In the low density limit, corresponding to an initial cell density below the limit of close packing and a low viscosity limit, the small wavelength cutoff disappears and the system is unstable at all wavelengths.

In model II the instability is driven by the effect of traction forces exerted by the cells on the substrate. One observes an instability at all wavelengths appearing for very high values of the traction force. Decreasing the traction force the system becomes stable at shorter wavelengths. Below a critical value of the cell traction the system is always stable. Depending on the choice of the functional dependence of the exerted force on the cell density one observes different scenarios. We considered as examples two model choices, characterized by either presence or absence of saturation of the exerted force at high density values. In both cases the system turns out to be stable at low densities. In the presence of saturation the system is stable also at very high densities.

2. **Analysis of Model I.** In the model proposed in [5] the population of endothelial cells in the early stages of its evolution is described as a fluid of non directly interacting particles. Cells are accelerated by gradients of soluble mediators and slowed down by friction due to the interaction with the fixed substratum. A chemotactic factor is released by the cells, diffuse and degrade in a finite time. A phenomenological, density dependent pressure $g(n)$, zero at low densities and rapidly increasing when cells become closely packed, controls cell overcrowding.

In the model, cellular matter is described by means of a continuum cell density field n and of the corresponding Eulerian velocity field $\mathbf{v}$. Cell proliferation is negligible in *in vitro* vasculogenesis experiments, so it is possible to assume that the two quantities n and $\mathbf{v}$ are linked by a continuity equation. The situation is in some sense half-way between that of a discrete and of a continuous model, since initial conditions used in the simulation of Fig. 1 are given in the form of a discrete set of Gaussian bumps of width of the order of the average cell diameter ($\sim 30\mu$m), placed at random position with uniform probability over a square surface. Along with the cell density field n, a concentration field c of chemotactic factor is considered. The chemotactic factor allows cells to exchange information about the respective positions. It is released by the cells themselves, and it diffuses in the surrounding medium creating a concentration landscape. Cells then move towards zones of higher concentration of the chemotactic factor. Cells directional persistence is modeled by means of an inertia term. This gives rise [5, 1] to an inviscid, Burgers-like equation [2, 15] for the cell motion, coupled to a diffusion equation for the chemotactic factor:

$$
\begin{cases}
\frac{\partial n}{\partial t} + \nabla \cdot (n\mathbf{v}) = 0, \\
\frac{\partial \mathbf{v}}{\partial t} + \mathbf{v} \cdot \nabla \mathbf{v} = \mu \nabla c - \beta \mathbf{v} + \gamma \nabla^2 \mathbf{v} - \nabla g(n), \\
\frac{\partial c}{\partial t} = D \nabla^2 c + a n - \tau^{-1} c,
\end{cases}
\tag{2.1}
$$

where D, a, τ are respectively the diffusion coefficient, the rate of release and the characteristic degradation time of the chemotactic factor. The parameter μ measures the strength of the cell response and β is a drag coefficient. Here we also consider a viscous term $\gamma \nabla^2 \mathbf{v}$. This term introduces an energy dissipation mechanism in the equations, which can be thought to model the slowing down of cells in the proximity of network structures. The viscous term is particularly relevant in the presence of high velocity gradients, as those observed during the process of pattern formation close to the network structures.

Burgers' equations is a well established paradigm in the theory of self-organized aggregation and pattern formation, which has been utilized to describe the emergency of structured patterns in many different settings [2,8,6,13,15]. In Burgers' equation matter in the earlier stages of its evolution is described as a free particle fluid [13]. The free particle fluid dynamics has the effect of strongly amplifying small inhomogeneities in the initial data. After a characteristic time, faster particles catch up slower ones and form a network of shock waves, which in two dimensions are strikingly similar to capillary-like networks [6,13]. The coupling with the diffusion equation for the chemoattractant factor introduces in the problem a natural length scale r_0, corresponding to the effective range of chemical interaction, which is finite because the chemoattractant factor is degraded by the medium in a finite, measurable time.[3] Numerical simulations [1,5] show that this natural length scale is responsible for the characteristic scale of formed network structures, which is a physiologically relevant feature of real vascular networks. The process of network formation is understood in the following way. Initially, non zero velocities are built up by the chemoattractive term due to the presence of random inhomogeneities in the density distribution. Then, the Burgers dynamics amplifies the inhomogeneities and forms a capillary-like network. Density inhomogeneities are translated in a landscape of concentration of the chemoattractant factor where details of scales r_0

---

[3]The half-life of the chemoattractant factor in usual experimental situations is of the order of one hour [5].

are averaged out. The cellular matter move toward the ridges of the concentration landscape. The Burgers dynamics sharpens the ridges and empties the valleys in the concentration landscape, eventually producing a network structure characterized by a length scale of order r_0. This way, the model provides a direct link between the structure dimensions and the range of intercellular interaction.

2.1. **Linear stability.** Linearizing Eqs. (2.1) around the uniform steady state $(n, \mathbf{v}, c) = (n_0, \mathbf{0}, a\tau n_0)$:

$$n = n_0 + \hat{n}, \quad \mathbf{v} = \hat{\mathbf{v}}, \quad c = a\tau n_0 + \hat{c}$$

one obtains the perturbation equations

$$\frac{\partial \hat{n}}{\partial t} + n_0 \nabla \cdot \hat{\mathbf{v}} = 0,$$

$$\frac{\partial \hat{\mathbf{v}}}{\partial t} = \mu \nabla \hat{c} - \beta \hat{\mathbf{v}} + \gamma \nabla^2 \hat{\mathbf{v}} - g'(n_0)\nabla \hat{n},$$

$$\frac{\partial \hat{c}}{\partial t} = D\nabla^2 \hat{c} + a\hat{n} - \frac{1}{\tau}\hat{c}.$$

By substituting

$$\hat{n} = n_0 n^*, \quad \hat{\mathbf{v}} = \sqrt{\mu a \tau n_0}\mathbf{v}^*, \quad \hat{c} = a\tau n_0 c^*, \quad t = \frac{\sqrt{D}}{\sqrt{\mu a n_0}}t^*, \quad \mathbf{x} = \sqrt{D\tau}\mathbf{x}^*$$

we obtain the dimensionless system

$$\begin{cases} \frac{\partial n^*}{\partial t^*} + \nabla \cdot \mathbf{v}^* = 0, \\ \frac{\partial \mathbf{v}^*}{\partial t^*} = \nabla c^* - \beta^* \mathbf{v}^* + \gamma^* \nabla^2 \mathbf{v}^* - g_0 \nabla n^*, \\ \epsilon \frac{\partial c^*}{\partial t^*} = \nabla^2 c^* + n^* - c^*, \end{cases} \qquad (2.2)$$

where

$$\beta^* = \beta \frac{\sqrt{D}}{\sqrt{\mu a n_0}}, \quad \gamma^* = \frac{\gamma}{\tau \sqrt{\mu a n_0 D}},$$

$$\epsilon = \tau \frac{\sqrt{\mu a n_0}}{\sqrt{D}}, \quad g_0 = \frac{1}{\mu a \tau}g'(n_0).$$

While the parameters β^*, γ^* and ϵ are all positive, g_0 can in principle assume negative values. However, if we make the reasonable assumption that $g(n)$ is a nondecreasing function of n, $g_0 \geq 0$. Expanding in normal modes

$$(n^*, \mathbf{v}^*, c^*) = (\bar{n}, \bar{\mathbf{v}}, \bar{c}) \exp\{\sigma t^* + i\alpha_x x^* + i\alpha_y y^*\}$$

we obtain

$$\begin{cases} \sigma \bar{n} + i[\alpha_x \bar{v}_x + \alpha_y \bar{v}_y] = 0, \\ \sigma \bar{v}_x - i\alpha_x \bar{c} + \beta^* \bar{v}_x + \gamma^* \alpha^2 \bar{v}_x + ig_0 \alpha_x \bar{n} = 0, \\ \sigma \bar{v}_y - i\alpha_y \bar{c} + \beta^* \bar{v}_y + \gamma^* \alpha^2 \bar{v}_y + ig_0 \alpha_y \bar{n} = 0, \\ \epsilon \sigma \bar{c} + \alpha^2 \bar{c} + \bar{c} - \bar{n} = 0, \end{cases}$$

where $\bar{\mathbf{v}} = (\bar{v}_x, \bar{v}_y)$ and $\alpha^2 = \alpha_x^2 + \alpha_y^2$. These equations can be rewritten in matrix form:

$$\mathbf{A}\mathbf{w} = \mathbf{0},$$

where $\mathbf{w} = (\bar{n}, \bar{v}_x, \bar{v}_y, \bar{c})^T$ and

$$\mathbf{A} = \begin{pmatrix} \sigma & i\alpha_x & i\alpha_y & 0 \\ ig_0\alpha_x & \sigma + \beta^* + \gamma^*\alpha^2 & 0 & -i\alpha_x \\ ig_0\alpha_y & 0 & \sigma + \beta^* + \gamma^*\alpha^2 & -i\alpha_y \\ -1 & 0 & 0 & \epsilon\sigma + 1 + \alpha^2 \end{pmatrix}.$$
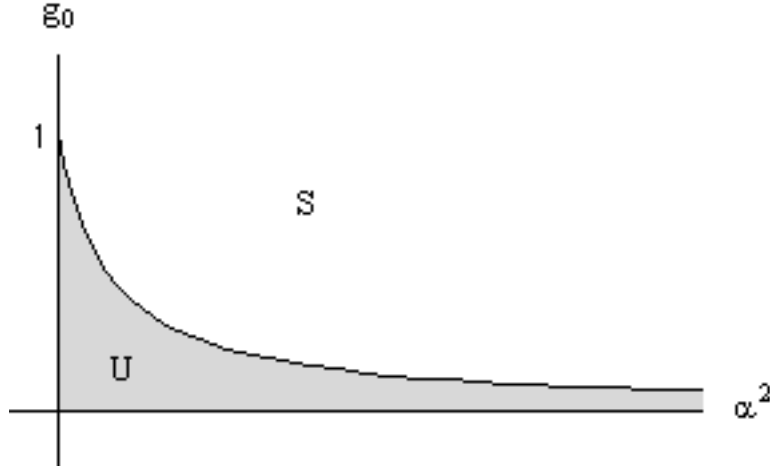
FIGURE 2. Stability (S) and instability (U) domains for system (2.2).

The determinant of the matrix $\mathbf{A}$ vanishes when

$$\det \mathbf{A} = (\sigma + \beta^* + \gamma^* \alpha^2) w(\sigma) = 0, \qquad (2.3)$$

where

$$w(\sigma) \;\; = \epsilon \sigma^3 + \sigma^2 \big(1 + \epsilon \beta^* + \alpha^2 (1 + \epsilon \gamma^*)\big) \\ + \sigma \big(\beta^* + \alpha^2 (\beta^* + \gamma^* + \epsilon g_0) + \alpha^4 \gamma^*\big) + \alpha^2 \big(g_0 (1 + \alpha^2) - 1\big). \qquad (2.4)$$

In addition to the negative growth rate $\sigma = -(\beta^* + \gamma^* \alpha^2)$, applying the Routh-Hurwitz theorem [3] one has the following necessary and sufficient conditions for the eigenvalues to have negative real parts:

$$\alpha^2 \big(g_0 (1 + \alpha^2) - 1\big) > 0,$$

$$\big(1 + \epsilon \beta^* + \alpha^2 (1 + \epsilon \gamma^*)\big)\big(\beta^* + \alpha^2 (\beta^* + \gamma^* + \epsilon g_0) + \alpha^4 \gamma^*\big) - \epsilon \alpha^2 \big(g_0 (1 + \alpha^2) - 1\big) > 0. \quad (2.5)$$

Rewriting Ineq. (2.5) in the form

$$\big(1 + \epsilon \beta^* + \alpha^2 (1 + \epsilon \gamma^*)\big)\big(\beta^* + \alpha^2 (\beta^* + \gamma^*) + \alpha^4 \gamma^*\big) + \epsilon^2 (\beta^* + \alpha^2 \gamma^*) \alpha^2 g_0 + \epsilon \alpha^2 > 0$$

it is trivial to realize that it is always satisfied. A sufficient condition for the stability of the stationary configuration is then given by

$$g_0 \geq 1. \qquad (2.6)$$

If instead $g_0 < 1$, the stationary configuration is unstable to perturbations with wave number

$$\alpha^2 < \frac{1 - g_0}{g_0}, \quad \text{or} \quad g_0 < \frac{1}{1 + \alpha^2} \qquad (2.7)$$

The corresponding region of instability is shaded in Fig. 2.

2.2. **Critical wave number.** In order to explicitly characterize the critical wavelength (*i.e.*, the faster growing mode), here and in the following section we consider the fast diffusion limit $\epsilon \ll 1$ of Eqs. (2.2). Setting $\epsilon = 0$ and proceeding as in the previous chapter we find a similar result and Eq. (2.4) replaced by

$$w(\sigma) = (1 + \alpha^2) \sigma^2 + \big(\beta^* + (\beta^* + \gamma^*) \alpha^2 + \gamma^* \alpha^4\big) \sigma + \big(g_0 (1 + \alpha^2) - 1\big) \alpha^2. \qquad (2.8)$$
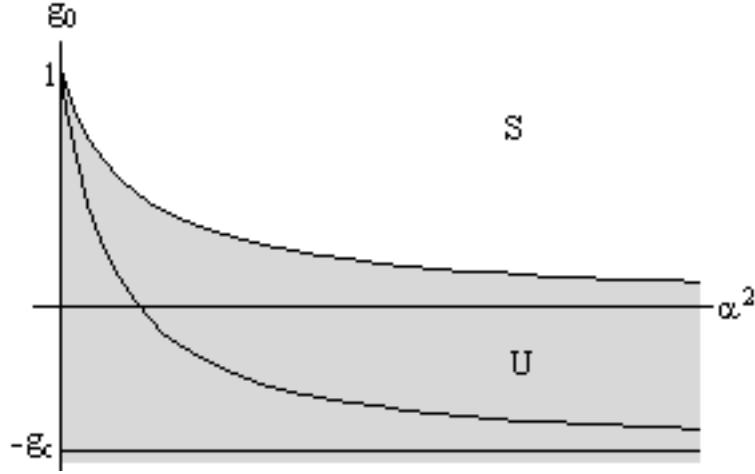
FIGURE 3. Stable (S) and unstable (U) regions for system (2.2) with $\epsilon = 0$. The lower curve $g_0(\alpha_R^2)$ encodes the relation between g_0 and the critical wave number α_R^2. Here $g_c = \gamma^*/\beta^*$

The instability condition is still given by Ineq. (2.7). The positivity of parameters β^* and γ^* implies that if $w(\sigma)$ has a complex root, then its real part is always negative. Thus the critical wave number is linked to real roots of Eq. (2.8). Looking for a maximum of $\sigma(\alpha^2)$ (i.e. imposing $d\sigma/d\alpha^2 = 0$) we obtain the equation

$$\sigma^2 + (\beta^* + \gamma^* + 2\gamma^*\alpha^2)\sigma + g_0(1 + 2\alpha^2) - 1 = 0. \tag{2.9}$$

Coupling it with $w(\sigma) = 0$ we obtain a relation between the critical wave number α_R^2 and $\sigma_c = \sigma(\alpha_R^2)$:

$$\sigma_c = \frac{1 - g_0\hat{\alpha}^2}{\gamma^*\hat{\alpha}^2}, \tag{2.10}$$

where $\hat{\alpha} = 1 + \alpha_R^2$ and $\gamma^* \neq 0$. Substituting (2.10) into Eq. (2.8) results in the equation for $\hat{\alpha}$:

$$(g_0^2 - g_0\gamma^*\beta^* - \gamma^{*2})\hat{\alpha}^4 + 2\gamma^{*2}\hat{\alpha}^3 + (\gamma^*(\beta^* - \gamma^*) - 2g_0)\hat{\alpha}^2 + 1 = 0. \tag{2.11}$$

Instead of determining α^2 as a function of g_0 it is easier to evaluate g_0 as a function of $\hat{\alpha}$. Taking into account the positivity of σ_c in Eq. (2.10) (see Ineq. (2.7)) we obtain g_0 explicitly:

$$g_0 = \frac{1}{2\hat{\alpha}^2}\left(\gamma^*\beta^*\hat{\alpha}^2 + 2 - \sqrt{(\gamma^*\beta^*\hat{\alpha}^2)^2 + (2\gamma^*\hat{\alpha}(\hat{\alpha} - 1))^2}\right), \tag{2.12}$$

The corresponding region of instability is shaded in Fig. 3.

2.3. **Limiting cases. a)** $g_0 = 0$.
The parameter g_0 is proportional to $g'(n_0)$ and therefore depends on the particular form of the function $g(n)$. This function was introduced in [5] to control cell over-crowding, and is flat (in fact zero) for low densities, *i.e.* for cell densities below the close-packing value n_s. It is therefore interesting to consider the $g_0 \to 0$ limit. Under this condition the uniform state turns out to be unstable to all wave numbers. In particular the most unstable mode is given by

$$-\gamma^{*2}\hat{\alpha}^4 + 2\gamma^{*2}\hat{\alpha}^3 + \gamma^*(\beta^* - \gamma^*)\hat{\alpha}^2 + 1 = 0,$$
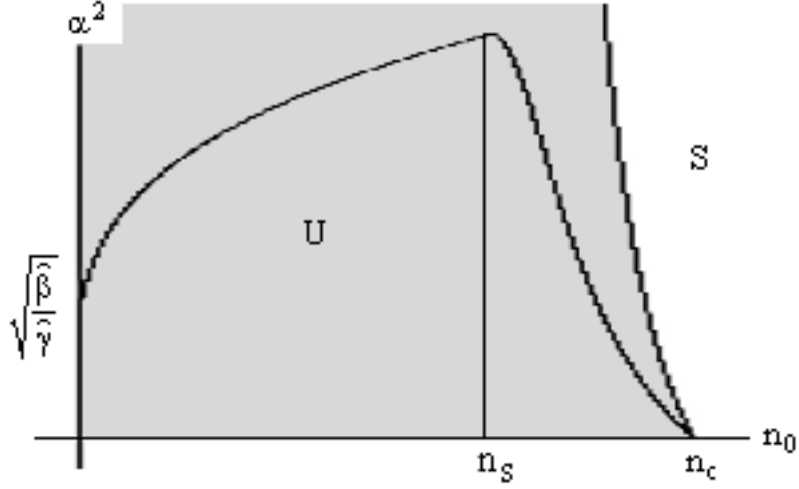
FIGURE 4. The critical wave number α_R^2 as a function of n_0 in the $g_0 = 0$ case. Here $\hat{\beta} = \hat{\gamma} = 0.1$. The point n_s is the close-packing value. The unstable region (U) is shaded.

which, recalling the definition of $\hat{\alpha}$ gives

$$\beta^* = \gamma^* \alpha_R^4 - \frac{1}{\gamma^*(1 + \alpha_R^2)^2}. \tag{2.13}$$

One has to take into account the fact that both parameters β^* and γ^* depend on n_0:

$$\beta^* = \frac{\hat{\beta}}{\sqrt{n_0}},$$

$$\gamma^* = \frac{\hat{\gamma}}{\sqrt{n_0}}.$$

Thus, Eq. (2.13) can be rewritten in the form

$$n_0 = \hat{\gamma}(\hat{\gamma}\alpha_R^4 - \hat{\beta})(1 + \alpha_R^2)^2. \tag{2.14}$$

The function $n_0(\alpha_R^2)$ in Eq. (2.14) is a convex increasing function with derivative at $n_0 = 0$ given by $2\sqrt{\hat{\beta}\hat{\gamma}}(\sqrt{\hat{\beta}} + \sqrt{\hat{\gamma}})^2$. Thus, looking at the inverse function $\alpha_R^2(n_0)$, one observes that for small values of the parameters $\hat{\beta}$, $\hat{\gamma}$ and for small density n_0, the critical wave number grows rapidly. On the other hand, in the domain $n > n_s$ ($g_0 > 0$ goes to infinity as n_0 tends to n_M) the critical wave number decreases and eventually vanishes in the point $n_c \in (n_s, n_M)$ such that $g(n_c) = 1$ (see Fig. 4).

b) $\gamma^* = 0$.

The viscosity term in the second equation of Model (2.2) (with $\epsilon = 0$) can be neglected in a first approximation. Let us therefore consider the $\gamma^* = 0$ limit of model (2.2). The corresponding characteristic polynomial is then:

$$\det \mathbf{A} = (1 + \alpha^2)(\sigma + \beta^*)w(\sigma),$$

where

$$w(\sigma) = \sigma^2 + \beta^* \sigma + g_0 \alpha^2 - \frac{\alpha^2}{1 + \alpha^2}. \tag{2.15}$$

The critical wave number is then given by

$$\frac{d\sigma}{d\alpha^2} = 0 \implies \alpha_R^2 = \frac{1}{g_0} - 1, \tag{2.16}$$

provided that $g_0 \neq 0$. The instability condition $(g_0 < 1)$ implies the positivity of α_R^2. The eigenvalue σ in the point α_R^2 is

$$\sigma_c = \sigma(\alpha_R^2) = \frac{1}{2}\left(-\beta^* + \sqrt{\beta^{*2} + 4\left(1 - \sqrt{g_0}\right)^2}\right)$$

is obviously positive and is bounded from above by the value $\sigma_M = \frac{1}{2}(-\beta^* + \sqrt{\beta^{*2} + 4})$.

It is interesting to check what happens when one imposes the further condition $g_0 = 0$. Eq. (2.15) shows that the main instability is at short waves. The eigenvalue $\sigma(\alpha_R^2)$ is however still bounded by the threshold σ_M, corresponding to the fact that cells tend to aggregate on the smaller scale possible.

3. **Analysis of Model II.** The model introduced in [10] focuses on the interaction of the cell network with an underlying, deforming substratum. Let $n(t, x)$ be the number of cells per unit area and $\rho(t, x)$ the substratum density. The vector $\mathbf{u}(t, \mathbf{x}) = (u_1(t, \mathbf{x}), u_2(t, \mathbf{x}))$ denotes the displacement of the substratum from its natural configuration. Under the assumption that there is no substratum production, local changes in the substratum density only occur because of convection:

$$\frac{\partial \rho}{\partial t} + \nabla \cdot (\rho \mathbf{v}) = 0, \tag{3.1}$$

where the velocity of the substratum is linked to its displacement by $\mathbf{v} = d\mathbf{u}/dt$. The cell density changes are instead described by

$$\frac{\partial n}{\partial t} + \nabla \cdot (n\mathbf{v}) = D\nabla^2 n, \tag{3.2}$$

where it is assumed that cells diffuse while they are pulled by the fibers of the substratum. The term $\nabla \cdot (n\mathbf{v})$ represents the convective flux, as the cells ride passively on the substratum.

The force balance equation of the system is

$$0 = \nabla \cdot \mathbf{T} + \nabla f(n) - \frac{s}{h(\rho)}\mathbf{v}, \tag{3.3}$$

because inertial effects are negligible compared to the viscous and other forces present in the system. The stress tensor $\mathbf{T}$ in the r.h.s. of Eq. (3.3), which originates due to the response of the substratum fibers to traction by cells, is given by the following constitutive equation

$$\Lambda\frac{\partial \mathbf{T}}{\partial t} + \mathbf{T} = \frac{E}{1+\nu}\left[\mu_1\frac{\partial \epsilon}{dt} + \mu_2\frac{\partial \theta}{dt}I + \epsilon + \frac{\nu}{1-2\nu}\theta I\right], \tag{3.4}$$

where E is Young's modulus, ν is the Poisson ratio, Λ is the relaxation time and μ_1, μ_2 are the shear and bulk retardation times. The tensor $\epsilon = \frac{1}{2}(\nabla\mathbf{u} + (\nabla\mathbf{u})^T)$ and the scalar function $\theta = \nabla \cdot \mathbf{u}$ denote respectively the strain and dilation. The function $f(n)$ represents the traction forces exerted by the cells on the substratum. The last term in the r.h.s. of Eq. (3.3) represents the external force due to the fact that the substratum deformation induced by cell traction is opposed by the anchoring of the substratum on the Petri dish (s is a drag coefficient, while $h(\rho)$ is a function of the substratum thickness).

3.1. **Linear stability.** Linearizing Eqs. (3.1–3.4) around the uniform state $(\rho, n, \mathbf{u}, \mathbf{T}) = (\rho_0, n_0, \mathbf{0}, \mathbf{0})$:

$$\rho = \rho_0 + \hat{\rho}, \quad n = n_0 + \hat{n}, \quad \mathbf{u} = \mathbf{0} + \hat{\mathbf{u}}, \quad \mathbf{T} = \mathbf{0} + \hat{\mathbf{T}} \qquad (3.5)$$

one obtains the following perturbation equations

$$\begin{cases} \frac{\partial \hat{\rho}}{\partial t} + \rho_0 \nabla \cdot \hat{\mathbf{v}} = 0 \,, \\ \frac{\partial \hat{n}}{\partial t} + n_0 \nabla \cdot \hat{\mathbf{v}} = D_0 \nabla^2 \hat{n} \,, \\ \frac{s}{h(\rho_0)} \hat{\mathbf{v}} = \nabla \cdot \hat{\mathbf{T}} + f'(n_0) \nabla \hat{n} \,, \\ \Lambda \frac{\partial \hat{\mathbf{T}}}{\partial t} + \hat{\mathbf{T}} = \frac{E}{1+\nu} \left[\mu_1 \frac{\partial \epsilon}{\partial t} + \mu_2 \frac{\partial \theta}{\partial t} I + \epsilon + \frac{\nu}{1-2\nu} \theta I \right] , \end{cases} \qquad (3.6)$$

where $\hat{\mathbf{v}} = \partial \hat{\mathbf{u}}/\partial t$. The first equation of system (3.6) has no influence on the stability analysis and can be omitted. In addition, ρ only appears in the third equation through the evaluation of the function h in ρ_0. So the particular choice of the function h has no effect on the linear stability result. We introduce the dimensionless variables:

$$n^* = \frac{\hat{n}}{n_0}, \quad \mathbf{u}^* = \frac{\hat{\mathbf{u}}}{\sqrt{D_0 T}}, \quad t^* = \frac{t}{T}, \quad x^* = \frac{x}{\sqrt{D_0 T}}, \quad \mathbf{T}^* = \hat{\mathbf{T}} \frac{1+\nu}{E},$$

where the characteristic time scale is assumed to depend on the sum of retardation times, i.e. $T = \frac{\mu_1 + \mu_2}{1+V}$, where $V = \frac{\nu}{1-2\nu}$. One then has

$$\begin{cases} \frac{\partial n^*}{\partial t^*} + \nabla \cdot \frac{d\mathbf{u}^*}{dt^*} = \nabla^2 n^* \,, \\ S(1+V)\frac{d\mathbf{u}^*}{dt^*} = \nabla \cdot \mathbf{T}^* + F_0(1+V)\nabla n^* \,, \\ \Lambda_0 \frac{\partial \mathbf{T}^*}{\partial t^*} + \mathbf{T}^* = \lambda_1(1+V)\frac{\partial \epsilon^*}{\partial t^*} + \lambda_2(1+V)\frac{\partial \theta^*}{\partial t^*} I + \epsilon^* + V\theta^* I \,, \end{cases} \qquad (3.7)$$

where

$$S = \frac{sD_0(1+\nu)(1-2\nu)}{h(\rho_0)E(1-\nu)}, \quad F_0 = f'(n_0)n_0 \frac{(1+\nu)(1-2\nu)}{E(1-\nu)}, \quad \Lambda_0 = \Lambda \frac{1+V}{\mu_1 + \mu_2}$$

and

$$\lambda_i = \frac{\mu_i}{\mu_1 + \mu_2}.$$

From non-Newtonian fluid mechanics it is known that $\Lambda_0 < 1$. Expanding in normal modes

$$(n^*, \mathbf{u}^*, \mathbf{T}^*) = (\bar{n}, \bar{\mathbf{u}}, \bar{\mathbf{T}}) \exp\{\sigma t^* + i\alpha_x x^* + i\alpha_y y^*\}$$

and proceeding as in Section 2, one obtains the following eigenvalue problem

$$\mathbf{A} \begin{pmatrix} \bar{n} \\ \bar{u}_1 \\ \bar{u}_2 \end{pmatrix} = \mathbf{0}$$

with $\mathbf{A} = (a_{ij})_{i,j=1,2,3}$, where

$$\begin{aligned} a_{11} &= \sigma + \alpha^2 \\ a_{12} &= i\sigma \alpha_x \\ a_{13} &= i\sigma \alpha_y \\ a_{21} &= -2iF_0(1+V)C\alpha_x \\ a_{22} &= 2S(1+V)C\sigma + A\alpha^2 + (A+B)\alpha_x^2 \\ a_{23} &= (A+B)\alpha_x \alpha_y \\ a_{31} &= -2iF_0(1+V)C\alpha_y \\ a_{32} &= (A+B)\alpha_x \alpha_y \\ a_{33} &= 2S(1+V)C\sigma + A\alpha^2 + (A+B)\alpha_y^2 \end{aligned}$$

and
$$A = \sigma\lambda_1(1 + V) + 1, \quad B = 2(\sigma\lambda_2(1 + V) + V), \quad C = (\Lambda_0\sigma + 1).$$
Nontrivial solutions only exist when
$$\det \mathbf{A} = p(\sigma)q(\sigma) = 0, \tag{3.8}$$
where
$$p(\sigma) = 2S(1 + V)\Lambda_0\sigma^2 + (2S + \lambda_1\alpha^2)(1 + V)\sigma + \alpha^2$$
is a second order polynomial with both roots having negative real parts, and
$$q(\sigma) = J\sigma^3 + K\sigma^2 + L\sigma + M$$
is a third order polynomial with the following coefficients
$$J = \Lambda_0 S,$$
$$K = \alpha^2 + S + (S - F_0)\Lambda_0\alpha^2,$$
$$L = (\alpha^2 + 1 + S - F_0)\alpha^2,$$
$$M = \alpha^4.$$
The stability conditions for the stationary configuration then follow from the Routh-Hurwitz theorem [3]:
$$\alpha^2 > 0,$$
$$\alpha^2(1 + (S - F_0)\Lambda_0) + S > 0,$$
$$\alpha^4\big(1 + (S - F_0)\Lambda_0\big) + \alpha^2\big((1 + (S - F_0)\Lambda_0)(1 + S - F_0) + S(1 - \Lambda_0)\big) + S(1 + S - F_0) > 0.$$
Therefore the stationary state is stable if and only if
$$F_0 < F_c \equiv 1 + S.$$

3.2. **Critical wave number.** In order to obtain an explicit expression for the critical wave number we now set $\Lambda_0 = 0$. In this case, in equation (3.8) $J = 0$ and K, M are nonnegative for any value of the parameters. Therefore if $L^2 - 4KM \geq 0$, σ is real and the steady solution is stable if and only if $L > 0$, *i.e.*
$$F_0 < F_c + \alpha^2. \tag{3.9}$$
In the $L^2 - 4KM < 0$ case, i.e. when
$$\alpha^2 \in (\alpha_1^2, \alpha_2^2), \tag{3.10}$$
with
$$\alpha_1^2 = \max\left\{0, 1 + F_0 - S - 2\sqrt{F_0}\right\} \quad \text{and} \quad \alpha_2^2 = 1 + F_0 - S + 2\sqrt{F_0},$$
the real part of σ is still determined by the sign of L, i.e. by the stability condition (3.9). It follows that independently of the sign of the term $L^2 - 4KM$, the uniform state is stable for $F_0 < F_c$. If instead $F_0 > F_c$ the stationary configuration is unstable to long waves
$$\alpha^2 < F_0 - F_c. \tag{3.11}$$
From now on we restrict our analysis to the instability region in which (3.11) is fulfilled. It is trivial to check that for $F_0 > F_c$ the neutral stability curve is in the region identified by (3.10), so that the part of the instability domain with complex eigenvalues is defined by
$$\alpha^2 \in \left(\alpha_1^2, F_0 - F_c\right) \tag{3.12}$$
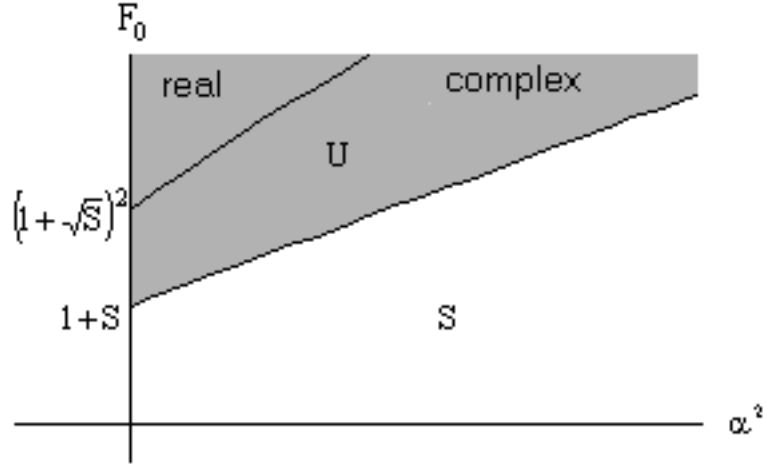provided that $F_0 > 1 + S$ (See Fig. 5).

FIGURE 5. Stable (S) and unstable (U) region for system (3.6). The instability region is divided in two parts, one corresponding to real and one corresponding to complex eigenvalues.

In this domain one can study the derivative of the real part of the σ eigenvalue:

$$\frac{\partial Re\sigma}{\partial \alpha^2} > 0 \iff \alpha^4 + 2S\alpha^2 - (F_0 - F_c)S < 0.$$

in order to find the critical wave number in the domain (3.12) and determine that $Re(\sigma)$ increases in the complex instability region for

$$\alpha^2 \leq \alpha_c^2, \tag{3.13}$$

where

$$\alpha_c^2 = -S + \sqrt{S(F_0 - 1)} \tag{3.14}$$

is a positive number. One notices that Ineq. (3.13) is relevant if $\alpha_c^2 \geq \alpha_1^2$, i.e. if

$$S \geq \frac{(\sqrt{F_0} - 1)^4}{F_0 - 1}. \tag{3.15}$$

Otherwise, in the same region the maximal $Re(\sigma)$ occurs for the mode $\alpha^2 = \alpha_1^2$. However one can deduce that α_c^2 is the global most unstable mode when $\alpha_1^2 = 0$, i.e. for

$$F_0 < (1 + \sqrt{S})^2. \tag{3.16}$$

In the region with real eigenvalues

$$\alpha^2 \in (0, \alpha_1^2) \tag{3.17}$$

the most unstable mode can be obtained by differentiating polynomial q in Eq. (3.8) (with $\Lambda_0 = 0$). The result is

$$\sigma^2 + (S + 1 - F_0 + 2\alpha^2)\sigma + 2\alpha^2 = 0. \tag{3.18}$$

The positive solution to the system of equations (3.8) and (3.18) is given by

$$\sigma_R = S + F_0 - 1 - 2\sqrt{SF_0} \tag{3.19}$$

and

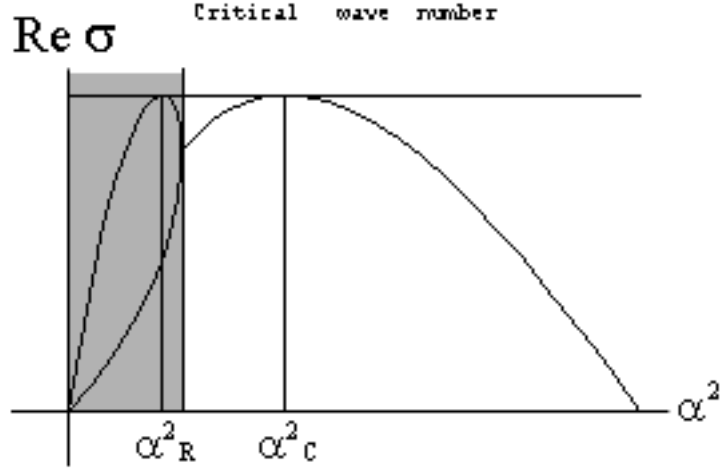$$\alpha_R^2 = \frac{\sqrt{S}[(\sqrt{F_0} - \sqrt{S})^2 - 1]}{\sqrt{F_0} - \sqrt{S}}. \tag{3.20}$$

FIGURE 6. Critical wave numbers α_R^2 and α_c^2 corresponding to the parameter values $F_0 = 9$ and $S = 3.01611$. Two branches of real solutions are shown in the shaded part of the graph, whereas in the other half of the graph the real part of the complex solution is drawn. For this particular values of the parameters σ_c and σ_R are equal.

Taking into account that $\sigma(0) = 0$ and that $\sigma(\alpha_R^2) > \sigma(\alpha_1^2)$, which can be easily checked, and noticing that the solution to Eq. (3.8) is a C^1 function in the domain (3.17), one can state that $\sigma(\alpha^2)$ has its maximum in the point α_R^2. Summarizing,
• if $F_0 < (1 + \sqrt{S})^2$, the most unstable mode is α_c^2,
• if $F_0 > (1 + \sqrt{S})^2$ and $S < \frac{(\sqrt{F_0}-1)^4}{F_0-1}$, then the most unstable mode is α_R^2,
• in the remaining region one has to compare the value $\sigma_c = \mathrm{Re}(\sigma(\alpha_c^2))$ with σ_R as done in Fig. 6.
One has
$$\sigma_R < \sigma_c \iff S \in (S_-, S_+), \tag{3.21}$$
where
$$S_\pm = \left(\sqrt{\sqrt{F_0}} \pm \sqrt{\sqrt{F_0} - \sqrt{F_0 - 1}} \right)^4$$
and
$$S_- > \frac{(\sqrt{F_0} - 1)^4}{F_0 - 1}.$$
It can be shown that $S_+ > F_0 - 1$ (our analysis is restricted to the region where $F_0 > 1 + S$). Thus α_R^2 is the critical wave number if and only if the following conditions are fulfilled:
$$F_0 > F_c + 2\sqrt{S} \quad \text{and} \quad S < S_-.$$
However it can be easily checked that the second inequality implies the first one. Thus, summing up all the obtained results, it turns out that the wave number α_R^2 is the most unstable mode if and only if
$$S < \left(\sqrt{\sqrt{F_0}} - \sqrt{\sqrt{F_0} - \sqrt{F_0 - 1}} \right)^4. \tag{3.22}$$
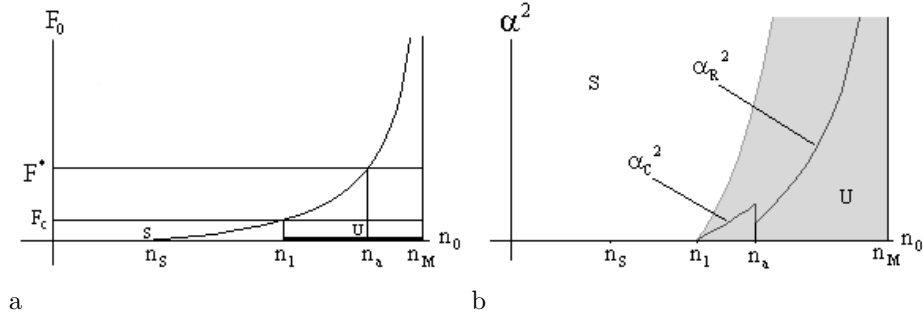
FIGURE 7. a: Instability condition for a function $f(n)$ with a blowup in $n = n_M$. For $n > n_1$ the solution is unstable. F^* denotes the value of F_0 where Ineq. (3.22) changes sign. b: The instability region (shaded). Both critical wave numbers α_c^2 and α_R^2 are indicated.

If Ineq. (3.22) is not satisfied, the mode α_c^2 is the critical one. One can also notice that in the interval $S \in [0, F_0 - 1)$, both σ_R and σ_c are decreasing functions of S. Moreover $\sigma_R(S_-) = \sigma_c(S_-)$. Thus, with fixed F_0 it turn out that $\sigma(S)$ takes its maximal value in $S = 0$ (in this case $\sigma_{max} = F_0 - 1$). On the other hand, with fixed S, it turns out that both σ_R and σ_c are increasing functions of $F_0 > 1 + S$ with $\sigma_R(F_0)$ tending to $+\infty$ as F_0 goes to $+\infty$.

3.3. **Dependence on the stationary cell density.** It should be remarked that the stability results strongly depend on F_0, which is proportional to $f'(n_0)n_0$ and therefore depends on the function $f(n)$. It is then useful to represent the results in terms of n_0. Let us first consider $f(n)$ to be a convex function, blowing up in correspondence of the value n_M and vanishing for $n < n_s$ (see Fig. 7a). This corresponds to the assumption that close packed cells exert a very high stress. The stability and instability regions corresponding to this choice of $f(n)$ are shown in Fig. 7a. Notice that there are points n_1 and n_a, such that for any $n_0 \in (n_1, n_a)$ the critical wave number is given by α_c^2, while for any $n > n_a$ the critical wave number is α_R^2. One can also describe the instability condition through the functional dependence of α^2 on n_0 (see Fig. 7b). The uniform distribution of cells is then stable when its density is lower than a critical value n_1. In particular it is stable when $n < n_s$ i.e. when the cell density is less than the close-packing value n_s (in such a case no stress is exerted by cells and $F_0 = 0$). At the onset of instability the distribution is unstable for very long waves.

In [10] the following function was considered:

$$f(n) = \tau \frac{n}{1 + an^2}. \tag{3.23}$$

corresponding to the assumption that the stress exerted by closely packed cells reaches a maximum in the density n and decreases for very high densities. In this case, if the maximum of $f'(n_0)n_0$ is not large enough (i.e. if $F_0 < 1 + S$) then the uniform distribution is always stable. Otherwise, referring to Fig. 8a, for any $n_0 \in (n_1, n_2)$ the uniform distribution is unstable. One can notice that if F^* (the point where Ineq. (3.22) changes its sign) is less then the maximal value of F_0 then there exist an interval (n_a, n_b), such that the critical wave number in this interval
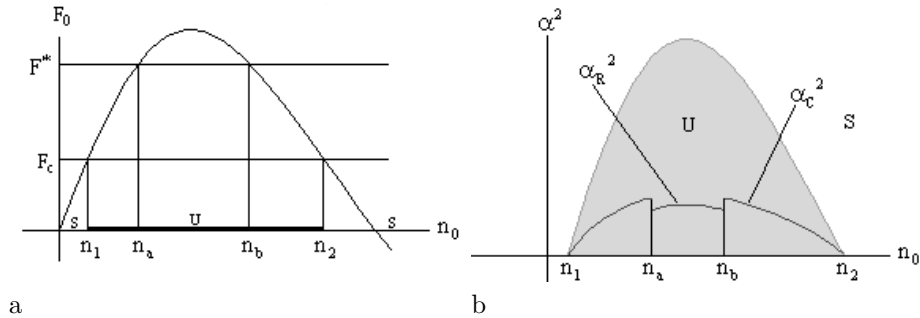
FIGURE 8. a: The instability condition corresponding to the choice (3.23) of $f(n)$. b: The instability region (shaded). The critical wave numbers α_c^2 and α_R^2 are indicated.

is given by α_R^2 (see Fig. 8b). At the onset of instability on both sides the uniform distribution is unstable for very long waves.

4. **Conclusions.** We considered two models of *in vitro* vasculogenesis. We performed a linear stability analysis around a uniform distribution of the two dimensional cell density, with the aim of checking their potential for structure formation starting from initial data representing a continuum cellular monolayer. For this kind of initial data, the main stabilizing force for Model I is pressure. Since pressure is assumed to be zero at low cell densities, and rapidly increasing above the close packing value, the system is unstable at low densities and stabilizes at higher densities. In the second model the instability is driven by the traction force exerted by cells on the substratum. The stability of the model strongly depends on the choice of the functional relation between the exerted force and the cell density. Starting from the reasonable assumption that at low densities there correspond low forces, one finds that the system is stable at low densities. In this respect we think that Model I better describe the Swiss-cheese transition shown in Figure 1, which is related to an instability at low densities and stability at high densities. In Model II stability at higher densities with an intermediate stability region can be recovered if the pulling force saturates at increasing densities, otherwise the model is always unstable at high densities.

We have thus enucleated in detail the conditions that lead to the appearance of instabilities in the two models. We expect that this information will be useful for further comparison with experiments.

The two models considered in this paper provide complementary description of *in vitro* vasculogenesis experiments. Model I succesfully describes the early, migration dominated stages of network formation observed in experiments performed with human endothelial cells [1]. In it simplest form, the model depends on parameters which either have been measured in real experimental conditions (the diffusion factor D and the chemoattractant half-life τ) or are in principle measurable (like the rate of release of chemoattractant or the pressure force exerted by closely packed cells). Moreover, the main theoretical prediction of the model, *i.e.* the average size of formed network structures, depends only on the two experimentally measured parameters and is in good agreement with observations.

Model II starts from physical premises which are not compatible with the description of the experiments performed in [1]: cell movement is assumed to be diffusive, while in [1] cells are observed to perform directed motions. The phenomenon of pattern formation in Model II has been shown starting from monolayer initial conditions, but not from the sparse initial conditions observed in [1]. Moreover, pattern formation in Model II critically depends on the *ad hoc* choice of the function (3.23), representing traction forces exerted by cells on the substratum. However, Model II is interesting because it describes a viscoelastic regime which is not accessible by Model I, and which becomes relevant as soon as the early migration stage ends and the network structure is formed. On the biological side, migration and traction can be considered as different programs that an individual cell is able to execute. One can argue that the start of either program is dictated by the environment, *e.g.* by the fact that the cell is isolated or among a closely packed group of other cells. So, different initial conditions can put the system either in a migrating or in a viscoelastic regime, thus explaining the different phenomenologies that inspired Models I and II.

It can be argued that a complete, realistic description of the diverse phases of *in vitro* vasculogenesis should consist in suitably connecting the migration regime described by Model I and the successive viscoelastic regime described by Model II or by some modification of it.

REFERENCES

[1] G. Serini, D. Ambrosi, E. Giraudo, A. Gamba, L. Preziosi, F. Bussolino. *Modeling the early stages of vascular network assembly,* EMBO J. **22** (2003), 1771.

[2] J. Burgers. "The Nonlinear Diffusion Equation," D. Reidel Publishing Co., Dordrecht, 1974.

[3] W. A. Coppel, "Stability and Asymptotic Behaviour of Differential Equations," Heath Mathematical Monographs, 1965.

[4] J. Folkman and C. Haudenschild. *Angiogenesis in vitro.* Nature **288** (1980), 551.

[5] A. Gamba, D. Ambrosi, A. Coniglio, A. de Candia, S. Di Talia, E. Giraudo, G. Serini, L. Preziosi, F. Bussolino. *Percolation, morphogenesis, and Burgers dynamics in blood vessels formation,* Phys. Rev. Lett. **90** (2003), 118101.

[6] S.N. Gurbatov, A.N. Malakhov, and A.I. Saichev. "Non linear random waves and turbulence in nondispersive media: waves, rays, particles," Manchester Un. Press, 1991.

[7] G. Helmlinger, M. Endo, N. Ferrara, L. Hlatky, and R.K. Jain. *Formation of endothelial cell networks,* Nature **405** (2000), 139–141.

[8] Y. Kuramoto. "Chemical Oscillations, Waves and Turbulence," Springer, Berlin, 1984.

[9] L.D. Landau and E.M. Lifshifts. "Fluid Mechanics," Pergamon Press, London, 1959.

[10] D. Manoussaki, S. R. Lubkin, R. B. Vernon and J. D. Murray. *A mechanical model for the formation of vascular networks in vitro,* Acta Biotheoretica **44** (1996), 271–282; J.D. Murray, D. Manoussaki, S.R. Lubkin and R.B. Vernon. *A mechanical theory of in vitro vascular network formation,* in "Vascular Morphogenesis: In Vivo, In Vitro and In Mente" (eds. C. Little, V. Mironov, H. Sage), Birkhäuser, 1998.

[11] W. Risau and I. Flamme. *Vasculogenesis,* Annu Rev. Cell Dev. Biol. **11** (1995), 73–91.

[12] D. Stauffer and A. Aharony. "Introduction to Percolation Theory," Taylor and Francis, London, 1994.

[13] M. Vergassola, B. Dubrulle, U. Frisch, and A. Noullez. *Burgers' equation, Devil's staircases and the mass distribution for large-scale structures,* Astron. Astrophys. **289** (1994), 325–356.
[14] G.B. Whitham. "Linear and Nonlinear Waves," John Wiley, New York, 1974.
[15] W. Liu, Asymptotic behavior of solutions of time-delayed Burgers' equation, Discrete and Continuous Dynamical Systems: B, **2**, (2002) 47–56.

Received November 2002; revised June 2003.

E-mail address: `kowalc@calvino.polito.it`
E-mail address: `preziosi@polito.it`